The excitation of OH by H2 revisited – I: fine-structure resolved rate coefficients

J. Klos, Q. Ma, P. Dagdigian, Alexander M. Hoole, A. Faure, F. Lique

Monthly Notices
of the
ROYAL ASTRONOMICAL SOCIETY

MNRAS **471,** 4249–4255 (2017)
Advance Access publication 2017 August 2

doi:10.1093/mnras/stx1968

The excitation of OH by H_2 revisited – I: fine-structure resolved rate coefficients

J. Kłos,[1] Q. Ma,[2]★ P. J. Dagdigian,[2] M. H. Alexander,[1] A. Faure[3] and F. Lique[1,4]†

[1]*Department of Chemistry and Biochemistry, University of Maryland, College Park, MD 20742-2021, USA*
[2]*Department of Chemistry, The Johns Hopkins University, Baltimore, MD 21218-2685, USA*
[3]*UJF-Grenoble 1/CNRS, Institut de Planétologie et dAstrophysique de Grenoble (IPAG) UMR 5274, F-38041 Grenoble, France*
[4]*LOMC - UMR 6294, CNRS-Université du Havre, 25 rue Philippe Lebon, BP 1123, F-76063 Le Havre cedex, France*

Accepted 2017 July 28. Received 2017 July 28; in original form 2017 June 30

ABSTRACT

Observations of OH in molecular clouds provide crucial constraints on both the physical conditions and the oxygen and water chemistry in these clouds. Accurate modelling of the OH emission spectra requires the calculation of rate coefficients for excitation of OH by collisions with the most abundant collisional partner in the molecular clouds, namely the H_2 molecule. We report here theoretical calculations for the fine-structure excitation of OH by H_2 (both *para*- and *ortho*-H_2) using a recently developed highly accurate potential energy surface. Full quantum close coupling rate coefficients are provided for temperatures ranging from 10 to 150 K. Propensity rules are discussed and the new OH–H_2 rate coefficients are compared to the earlier values that are currently used in astrophysical modelling. Significant differences were found: the new rate coefficients are significantly larger. As a first application, we simulate the excitation of OH in typical cold molecular clouds and star-forming regions. The new rate coefficients predict substantially larger line intensities. As a consequence, OH abundances derived from observations will be reduced from the values predicted by the earlier rate coefficients.

Key words: molecular data – molecular processes – ISM: abundances.

1 INTRODUCTION

The hydroxyl radical (OH) was the first molecule detected at radio wavelengths in the interstellar medium (ISM) via its 18-cm (1.7 GHz) fine-structure line (Weinreb et al. 1963). Since then, through radio and far-infrared transitions, OH has been extensively observed towards interstellar clouds, star-forming regions, stellar envelopes, protoplanetary discs and external galaxies. Observations of OH provide, in particular, critical constraints on oxygen and water chemistry (e.g Goicoechea et al. 2011). OH fine and hyperfine transitions can be employed as a tracer of both the density (Cotten et al. 2012) and temperature (Ebisawa et al. 2015) of molecular clouds. In protostars, *Herschel* observations have revealed that OH emission originates from interstellar shocks (Wampfler et al. 2013). OH Zeeman measurements can also be used to measure the interstellar magnetic field strength (Crutcher 2012). Finally, as a reactive radical, OH plays an important role in the gas-phase chemistry of both hydrides (Gerin, Neufeld & Goicoechea 2016) and complex organic molecules (Shannon et al. 2013).

Rate coefficients for the collisional excitation of OH are crucially needed to accurately derive the OH abundance in molecular clouds from the observations (Roueff & Lique 2013). Consequently, there have been a number of calculations of the interaction potential between the OH($X^2\Pi$) radical and the hydrogen molecule, and, subsequently, of the necessary rate coefficients.

Because of the orbital degeneracy of OH in its ground-state Π electronic state, two potential energy surfaces (PESs) are required to characterize this interaction. Most calculations of rate coefficients prior to 1994 employed the PESs computed by Kochanski & Flower (1981). These PESs were calculated at a relatively small number of planar molecular orientations, where the two surfaces correspond to states of different reflection symmetry (A' and A''). Alternatively, Offer & van Hemert (1993) utilized a multiconfiguration self-consistent field method with corrections for the dispersion interaction to compute electronically adiabatic PESs even for geometries with no symmetry. To obtain the diabatic PESs needed for the scattering calculations, they directly calculated the adiabatic–diabatic transformation, expressed in terms of a coordinate-dependent mixing angle. Offer, van Hemert & van Dishoeck (1994, hereafter OHD94) employed the later PESs in quantum close-coupling calculations of both integral state-to-state and hyperfine resolved cross-sections and rate coefficients. OHD94 provided a review of earlier calculations of OH–H_2 PESs and rate coefficients.

★ Present address: Institute for Theoretical Chemistry, University of Stuttgart, Pfaffenwaldring 55, D-70569 Stuttgart, Germany
† E-mail: francois.lique@univ-lehavre.fr

Recently, Ma et al. (2014) carried out a new investigation of the interaction of OH($X^2\Pi$) with H_2. In this study, two methods for calculating the interaction were employed, namely multireference configuration interaction (MRCISD+Q) and explicitly correlated spin-restricted coupled cluster theory with inclusion of single, double, and (perturbatively) triple excitations [RCCSD(T)-F12a]. The former approach can be employed for any nuclear geometry while the latter requires a plane of symmetry so that the two OH–H_2 states have distinct reflection symmetry (A' or A'') (the same restriction that characterized the calculation of Kochanski & Flower 1981). The inclusion of triple excitations in the coupled-cluster calculation provides a more accurate treatment of electron correlation. Ma et al. (2014) showed that the coupled cluster calculations give an accurate description of the global OH–H_2 interaction, despite the restricted angular sampling.

Both sets of PESs computed by Ma et al. (2014) yielded dimer dissociation energies (D_0) in good agreement with experimental measurements by Loomis, Schwarz & Lester (1996). Moreover, over the collision energy range 75–155 cm^{-1} the state-to-state cross-sections for transitions out of the $j = 1.5\,F_1 f$ level computed with both sets of PESs were found by Schewe et al. (2015) to agree well with relative integral cross-sections determined in a molecular beam experiment that incorporated a state selected, Stark decelerated OH beam.

Here, we use the coupled cluster PESs of Ma et al. (2014) to generate a new set of rate coefficients for the rotational excitation of OH by H_2. Although the hyperfine-structure of OH is frequently resolved in spectral surveys of molecular clouds (Harju, Winnberg & Wouterloot 2000; Wampfler et al. 2011), we do not include it in the calculations reported here. We focus in this paper on the fine-structure resolved rate coefficients that are useful for the interpretation of observations where the hyperfine structure is not resolved or in which the use of the hyperfine statistical equilibrium approach of Keto & Rybicki (2010) is justified. Hyperfine-resolved rate coefficients will be presented in a forthcoming publication.

This paper is organized as follows. Section 2 describes briefly the dynamical calculations. In Section 3, we report state-to-state resolved cross-sections and rate coefficients for the collisional excitation of OH by H_2, and compare our calculated rate coefficients with previous OH–H_2 rate coefficients currently used for astrophysical modelling. In Section 4, we present a first astrophysical application of the present rate coefficients. Conclusions are given in Section 5.

2 THEORETICAL APPROACH

In this work we apply the exact quantum theory developed before (Offer & Flower 1990; OHD94; Groenenboom et al. 2009; Ma et al. 2014; Schewe et al. 2015) for the interaction and scattering of an open-shell molecule in a $^2\Pi$ electronic state with a closed-shell diatomic molecule. We consider scattering of rigid OH and H_2 molecules with bond lengths equal to the average value in their respective ground vibrational levels. The open-shell fine-structure of the hydroxyl radical is taken fully into account in the calculations. The scattering calculations are similar to those presented before by Schewe et al. (2015) but here on a more extended grid of collision energies. We used the $^2\Pi$-$^1\Sigma^+$ molecule–molecule scattering basis implemented in the Hibridon (2012) suite of scattering programs.

We also note that OH–H_2 collisions can lead to the formation of H_2O+H products. Since the barrier to this reaction is at least 2000 cm^{-1} (3000 K), the reaction is inefficient at and below room temperature (Wakelam et al. 2015). Thus, at low to moderate temperature, collisional energy transfer is the dominant relaxation process.

The OH ground $X^2\Pi$ electronic state is split into a lower (labelled F_1) and upper (F_2) spin-orbit manifold (see Huber & Herzberg 1979). In Hund's case (a), for a molecule such as OH with a negative spin-orbit constant, these correspond, respectively, to parallel and opposed values of the sum of the projection quantum numbers of electronic orbital and spin angular momenta ($\Omega = 3/2$ and $\Omega = 1/2$). Each rotational level j is further split into two, close-lying Λ-doublet levels of opposite parity p, which are labelled + and −. These labels indicate how the electronic wavefunction of the OH transforms with respect to the space-fixed inversion operation $\hat{i}^{SF}\psi = \pm\psi$. The spectroscopic parity index ϵ for the $^2\Pi$ state is related to the parity p by $\epsilon = p(-1)^{j-1/2}$. The states with $\epsilon = +1$ are labelled e and those with $\epsilon = -1$, f. We will use and designate the rotational levels of OH by j, Ω, and the parity p.

The channel energies were determined from the following spectroscopic parameters, for H_2 rotational constant $B_0 = 59.322\,cm^{-1}$ (Huber & Herzberg 1979); and for OH($X^2\Pi$, v = 0): rotational constant $B_0 = 18.548\,cm^{-1}$, spin-orbit coupling constant $A = 139.21\,cm^{-1}$ and Λ-doubling parameters $p_\Lambda = 0.2350\,cm^{-1}$ and $q_\Lambda = -0.0391\,cm^{-1}$. The spectroscopic constants for OH were taken from Mélen et al. (1995).

The scattering calculations were performed using the OH–H_2 RCCSD(T)-F12 PESs of Ma et al. (2014) on a grid of total energies (E_{tot}) divided into several ranges denoted as (E_{min}, E_{max}, dE) delimited by E_{min} and E_{max} and varying steps dE in cm^{-1}: (0, 100, 0.1), (100, 200, 0.2), (200, 300, 0.5), (300, 500, 1.0), (500, 700, 2.0), (700, 900, 5.0) and (900, 1500, 10.0). The quantum close coupling equations were solved using the hybrid propagator of Alexander and Manolopoulos starting from $R = 3.5\,a_0$ to $R = 100\,a_0$. The integral cross-sections were obtained by summing contributions from all partial waves up to total angular momentum J ranging from 25.5 for E_{tot} around 100 cm^{-1}, 55.5 for E_{tot} around 500 cm^{-1} up to 125.5 for the largest total energies considered in this work. The rotational basis contained channels with OH rotational quantum number $0.5 \le j \le 8.5$ and H_2 rotational quantum number $j_2 = 0$, 2, 4 for *para*-H_2 and $j_2 = 1$, 3 for *ortho*-H_2.

We performed convergence tests at different total energies and concluded that increasing the rotational basis with j to 9.5 and j_2 to 5 in the case of OH–*ortho*-H_2 did not significantly change the computed cross-sections. We refer the reader to the paper by Schewe et al. (2015) for the comparison of the calculated cross-sections using the new RCCSD(T)-F12 PES employed in this work to the cross-sections presented by OHD94, which were calculated using the PESs developed previously by Offer & van Hemert (1993).

3 RESULTS

3.1 Rate coefficients

State-to-state integral cross-sections (without hyperfine resolution) were computed for 20 OH initial levels up to the $^2\Pi_{1/2}$, $j = 9/2$, $p = +/-$ levels in collisions with *para*-H_2 and *ortho*-H_2 in their $j_2 = 0 - 2$ and $j_2 = 1 - 3$ states, respectively:

$$\mathrm{OH}(^2\Pi_\Omega, j, p) + \mathrm{H_2}(j_2) \rightarrow \mathrm{OH}(^2\Pi_{\Omega'}, j', p') + \mathrm{H_2}(j_2') \quad (1)$$

The corresponding rate coefficients were computed for the temperature range from 5 to 150 K as an average over the collision

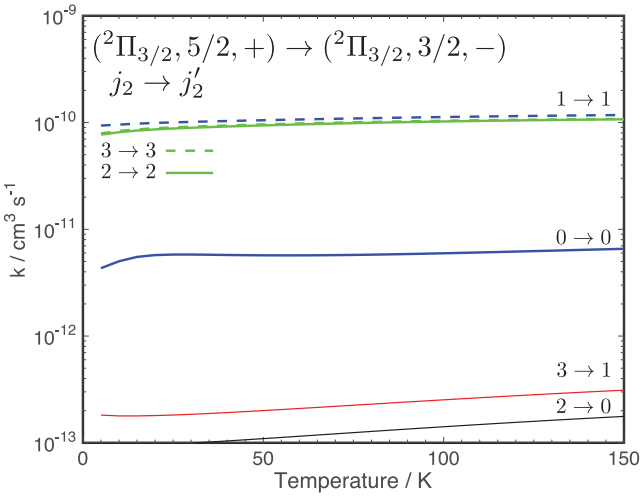

Figure 1. Comparison of rate coefficients for different rotational $j_2 \rightarrow j_2'$ transitions of H_2 molecule for selected OH transitions within the ground spin-orbit manifold.

energy (E_c):

$$k_{\alpha\rightarrow\beta}(T) = \left(\frac{8}{\pi\mu k_B^3 T^3}\right)^{\frac{1}{2}} \times \int_0^\infty \sigma_{\alpha\rightarrow\beta}\, E_c\, \exp\left(-\frac{E_c}{k_B T}\right) \mathrm{d}E_c \quad (2)$$

where $\sigma_{\alpha\rightarrow\beta}$ is the cross-section from the initial state α to the final state β, μ is the OH–H_2 reduced mass and k_B is Boltzmann's constant.

Fig. 1 shows the comparison of rate coefficients for the de-excitation of the $^2\Pi_{3/2}$, $j = 5/2$, $p = +$ rotational state to the ground rotational state for different initial and final rotational states of the *para*- and *ortho*-H_2 molecules.

One can notice that the rate coefficients for the de-excitations of the H_2 molecule, $j_2 = 2 \rightarrow j_2' = 0$ and $j_2 = 3 \rightarrow j_2' = 1$ are a factor of $\sim$100 smaller than rates for the cases where the H_2 molecule remains in the same rotational state.

For j_2-conserving transitions, the strong anisotropic interaction between the dipole moment of OH and the quadrupole moment of H_2 is responsible for the large rate coefficient for OH($^2\Pi_\Omega, j, p \rightarrow {}^2\Pi_{\Omega'}, j', p'$) – $H_2(j_2 = j_2')$ relaxation. However, in its $j_2 = 0$ level, the *para*-H_2 molecule is spherical and hence has no quadrupole moment. Thus, the $j_2 = 0 \rightarrow 0$ rate coefficients in Fig. 1 are much smaller.

For $j_2 > 1$, the rate coefficients for a given $^2\Pi_\Omega, j, p \rightarrow {}^2\Pi_{\Omega'}, j', p'$ transition are nearly independent of j_2. Consequently, hereafter, we will not discuss the relaxation of $H_2(j_2 = 3)$, since the rate coefficients are comparable to those for $j_2 = 2$.

In Fig. 2, we display temperature-dependent rate coefficients for selected de-excitation transitions of OH for spin-orbit conserving (left and middle columns) and spin-orbit changing (right column). These transitions correspond to as $\Delta j = j' - j = 1$ and $\Delta j = 2$ for the spin-orbit conserving transitions and $\Delta j = 0$ and $\Delta j = 1$ for the spin-orbit changing transitions.

In the top row panels labeled (a), (b) and (c), we showed OH rotational de-excitation transitions for collisions with *para*-H_2 in $j_2 = 0$ state for spin-orbit conserving $^2\Pi_{3/2} \rightarrow {}^2\Pi_{3/2}$, $^2\Pi_{1/2} \rightarrow {}^2\Pi_{1/2}$ and spin-orbit changing $^2\Pi_{1/2} \rightarrow {}^2\Pi_{3/2}$ transitions, respectively. The middle row panels (d), (e) and (f) of the figure present the same transitions but for the collisions with *ortho*-H_2 $j_2 = 1$ molecule. The bottom row shows transitions with the H_2 molecule in $j_2 = 2$ state in (g), (h) and (i) panels. The population of the $j_2 = 2$ rotational state becomes significant above $\sim$100 K (if *para*-H_2 is at thermal equilibrium).

The propensity rules that can be established looking at Fig. 2 are such that the $\Delta j = 2$ transitions are only prominent for collisions with $j_2 = 0$ *para*-H_2 shown in panel (a). For the other cases the rates with $\Delta j = 1$ are the largest ones. The rate coefficients for transitions that conserve the parity of the OH Λ-doublet level are the largest for collisions with *para*-$H_2(j_2 = 0)$ [panels (a)–(c)]. In the case of transitions in collisions with *ortho*-$H_2(j_2 = 1)$ the parity-changing rate coefficients tend to be the largest. It is also interesting to note that the rates for the spin-orbit changing transitions are comparable in magnitude to the spin-orbit conserving ones. For the transitions in collisions with *ortho*-$H_2(j_2 = 1)$ and *para*-$H_2(j_2 = 2)$, the differences between rates for the two Λ-doublet parities of the same initial rotational j_2 level are less pronounced than for transitions with *para*-$H_2(j_2 = 0)$. Again, this is likely a consequence of the absence of the dipole–quadrupole interaction in collisions with *para*-$H_2(j_2 = 0)$.

3.2 Comparison with previous results

As mentioned in the Introduction section, many collisional data sets are available for modelling OH emission from molecular clouds. For H_2 as a collision partner, the most recent is that of OHD94. This set is certainly the most used data set in astrophysical applications. Hence, we compare our new predicted rate coefficients. with those of OHD94. Fig. 3 shows this comparison for rate coefficients for all the de-excitation transitions between the first 20 fine-structure levels of OH. Results for both *para*-$H_2(j_2 = 0)$ and *ortho*-$H_2(j_2 = 1)$ colliding partners are shown.

As one can see, differences exist between the two sets of data. At low temperatures, the new rate coefficients are, on the average, higher than those of OHD94, the overall differences being a factor $\simeq$2–3. The new rate coefficients are, overall, larger than those of OHD94 for both *para*-$H_2(j_2 = 0)$ and *ortho*-$H_2(j_2 = 1)$. However, we note that the ratio between the two sets of data strongly depends on the transition considered and that, for some transitions, the OHD94 rate coefficients can be larger than the new ones. Such differences can be explained by the different well depths of the two PES used. While the overall dependence of the OHD94 and Ma et al. (2014) PESs upon the intermolecular separation and orientation is similar, the well depth of the OHD94 potential is deeper, as discussed by Ma et al. (2014). This leads to different expansion coefficients for the two PESs, and hence different magnitudes of the inelastic cross-sections. When the temperature increases, the overall differences between the two data sets decrease. However, the new data set remains globally larger than the old one by a factor of 1.5–2. In the light of these differences, and considering the high accuracy of the present data validated by comparison with the crossed beam experiments of Schewe et al. (2015), we recommend the use of our new rate coefficients in astrophysical applications.

4 THE EXCITATION OF OH IN THE ISM

As a first application and in order to test the impact of the new rate coefficients, we have performed radiative transfer calculations to simulate the excitation of OH in the ISM. As the hyperfine structure of the OH molecule was neglected in the scattering calculations, we focus in the following on pure rotational (fine-structure) lines and do not consider hyperfine substructure (see below).

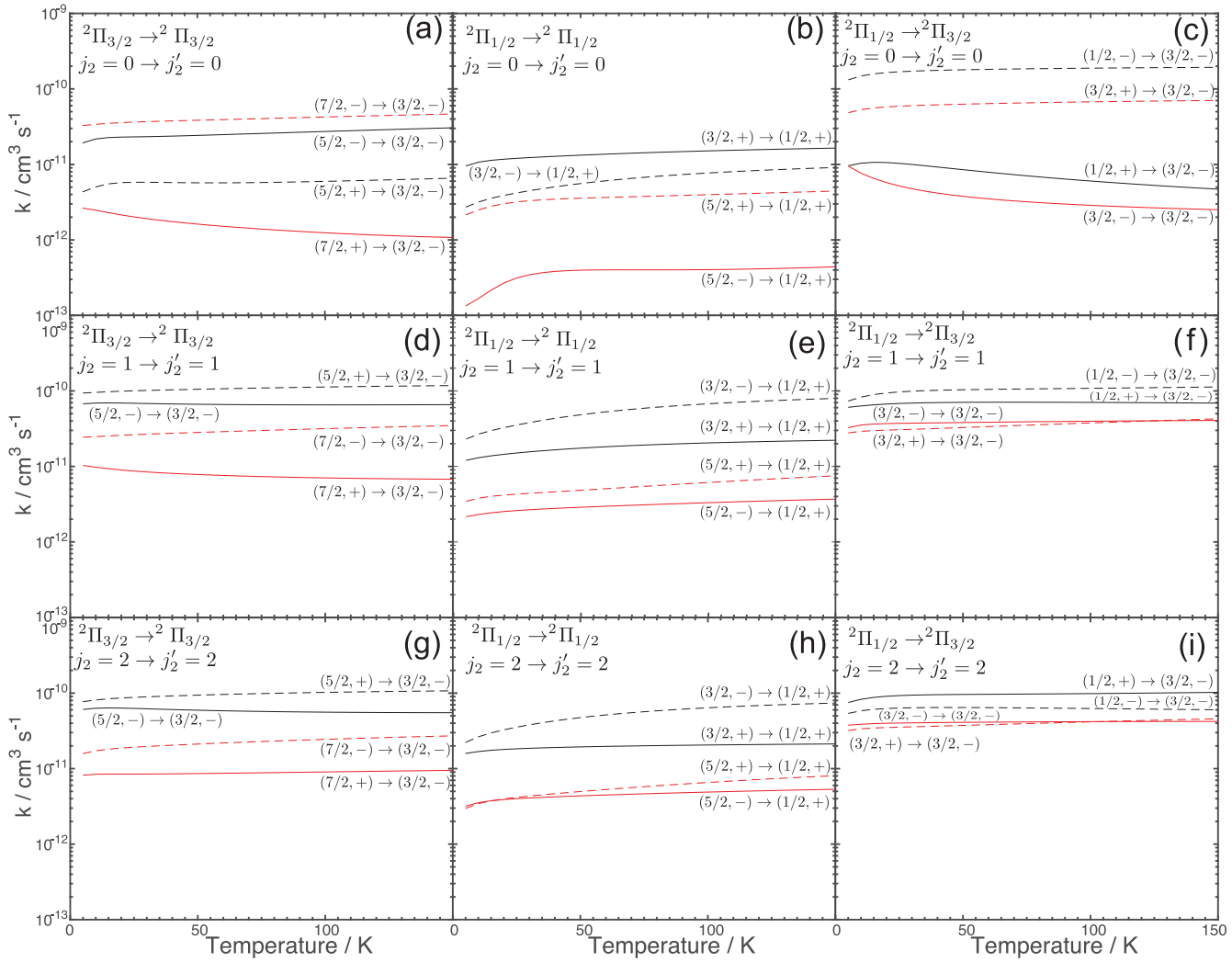

Figure 2. Temperature-dependent rate coefficients for a selected set of rotational transitions out of the OH in initial $j = 3/2$, 5/2, 7/2 states to the ground rotational state of the corresponding spin-orbit manifold ($j = 3/2, p = -$ for $^2\Pi_{3/2}$ and $j = 1/2, p = +$ for $^2\Pi_{1/2}$); see the text for details. The solid and dashed lines of the same colour correspond to the two Λ-doublet states with the same initial rotational quantum number j.

Non-local thermodynamic equilibrium (non-LTE) calculations were performed with the RADEX code (van der Tak et al. 2007) using the escape probability formalism approximation for an expanding sphere. We assume a uniform spherical geometry of the cloud. Both collisional and radiative processes are taken into account. We also include the cosmic microwave background (CMB) radiation at 2.73 K.

First, we focus on OH excitation in dense, cold molecular clouds. We consider a kinetic temperature of 10 K, OH column densities of 10^{14} or 10^{15} cm^{-2}, a line width of 1.0 km s^{-1} and a density of 3×10^4 cm^{-3}. Such physical parameters correspond to the typical physical conditions in dark clouds as, for example, in TMC-1 (Harju et al. 2000). At such low temperature only the Λ-doublet levels of the $^2\Pi_{3/2}, j = 3/2$ lowest state are significantly populated. Thus, only the $^2\Pi_{3/2}, j = 3/2, p = + \rightarrow {}^2\Pi_{3/2}, j = 3/2, p = -$ radiative transitions at 1.66 GHz can be detected.

We computed the brightness temperature for this transition using the new rate coefficients and those of OHD94. The brightness temperatures obtained from the two sets of data agree (not shown here) very well for the two column densities, despite the significant differences seen in the two sets of collisional data. This agreement can be explained by the fact that, at such density and temperature, the excitation temperature of this line approaches the kinetic temperature because of the very slow corresponding Einstein coefficient. Hence, in conditions where LTE is a good approximation, the impact of the new rate coefficients will be negligible in the analysis of OH emission spectra from cold molecular clouds.

Next, we focus on OH excitation in star-forming and protostellar regions. We consider a kinetic temperature of 100 K, an OH column density of 10^{16} cm^{-2}, a line width of 5.0 km s^{-1} and a density of 10^6 cm^{-3}. Such physical parameters correspond to those derived from the observation of OH in low- and intermediate-mass protostars and in star formation regions (Wampfler et al. 2013).

We computed the brightness temperature for a selected number of transitions using the new rate coefficients and those of OHD94. We consider both an *ortho-para* ratio of 0 (only *para*-H_2) and a thermal distribution of the two nuclear spin isomers (1.63 at 100 K). We consider eight transitions that are frequently observed (Wampfler et al. 2013), namely (a) four transitions within the $^2\Pi_{3/2}$ spin orbit manifold (the $^2\Pi_{3/2}, j = 5/2, p = +/- \rightarrow {}^2\Pi_{3/2}, j = 3/2$, $p = -/+$ transitions at 2509.95 and 2514.31 GHz and the $^2\Pi_{3/2}$,

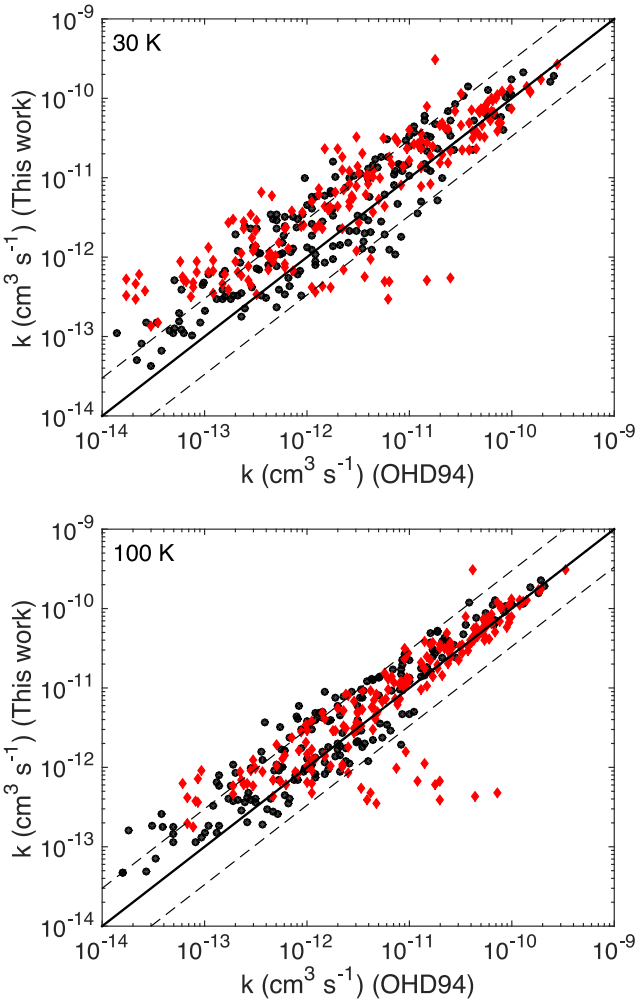

Figure 3. Comparison between rate coefficients predicted by the present calculations and those of OHD94 for all de-excitation transitions between the first 20 levels at 30 K (upper panel) and 100 K (lower panel). The vertical axis represents the OH–H_2 rate coefficients from this work and the horizontal axis represents the corresponding rate coefficients of OHD94. Both OH-*para*-H_2($j_2 = 0$) (filled black circles) and OH-*ortho*-H_2($j_2 = 1$) (filled red diamonds) results are presented. The two dashed lines in each panel delimit the region where the rate coefficients differ by less than a factor of 3.

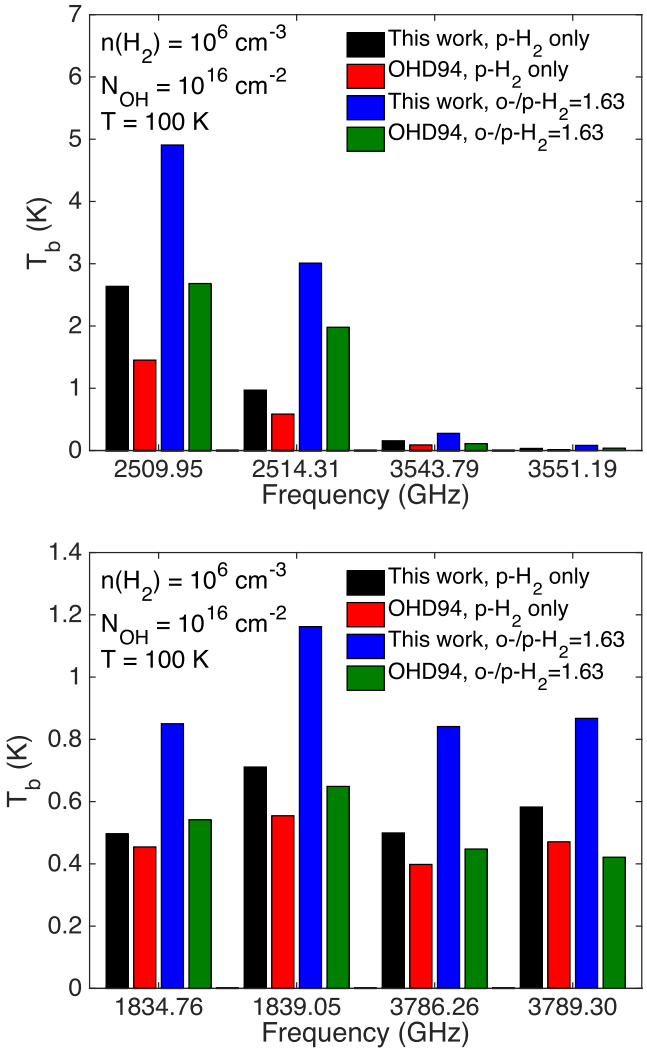

Figure 4. Brightness temperature (in K) of selected radiative transitions of OH for a kinetic temperature of 100 K and for a density of the collision partner of 10^6 cm^3 and an OH column density of 10^{16} cm^{-2}. Two sets of collisional rate coefficients are shown (this work versus OHD94). Two distributions of *ortho*-/*para*-H_2 colliders are considered: 0 and 1.63.

$j = 7/2$, $p = +/- \rightarrow {}^2\Pi_{3/2}$, $j = 5/2$, $p = -/+$ transitions at 3543.79 and 3551.19 GHz), (b) two transitions within the ${}^2\Pi_{1/2}$ spin orbit manifold (the ${}^2\Pi_{1/2}, j = 3/2, p = +/- \rightarrow {}^2\Pi_{1/2}, j = 1/2$, $p = -/+$ transitions at 1834.76 and 1839.05 GHz), and (c) two transitions between the two spin-orbit manifolds (the ${}^2\Pi_{1/2}, j = 1/2$, $p = +/- \rightarrow {}^2\Pi_{3/2}, j = 3/2, p = -/+$ transitions at 3786.26.95 and 3789.30 GHz). Fig. 4 shows the results of our radiative transfer calculations.

For all eight lines considered in this simulation and for the two data sets of collisional rate coefficients, one can see that the inclusion of o-H_2 increases the line intensities by up to a factor of 2. Such an increase has already been noticed by Offer & van Dishoeck (1992) and can be explained by the larger magnitude of the *ortho*-H_2 rate coefficients relative to the *para*-H_2 rate coefficients (related, as discussed above, to the absence of a quadrupole moment in the $j_2 = 0$ rotational level of H_2). It is thus crucial to know the *ortho*–*para* ratio of H_2 in the molecular clouds in order to accurately model OH emission spectra.

We also note that the line intensities obtained using the new rate coefficients are larger than those obtained using the OHD94 data, the line intensity ratios being $\simeq$2 for both choices of *ortho–para* ratio. The present calculations show that OH abundance derived from radiative transfer analysis performed using OHD94 rate coefficients are overestimates. The overestimation can reach a factor of 2. It is then crucial to use the new collisional data to revise the OH abundance in star-forming and protostellar regions.

We are also interested in the ${}^2\Pi_{3/2}$, $j = 3/2$, $p = + \rightarrow {}^2\Pi_{3/2}$, $j = 3/2$, $p = -$ fine structure line at 1.66 GHz that can be detected in warm star forming regions. Fig. 5 presents the excitation temperature and opacity of this line obtained with the new rate coefficients (solid lines) and OHD94 rate coefficients (dashed lines) as a function of density. We also used a kinetic temperature of 100 K, an OH column density of 10^{16} cm^{-2} and a line width of 5.0 km s^{-1}.

In contrast to what was found for cold molecular clouds, the excitation temperature of the line at 1.66 GHz is well below the kinetic

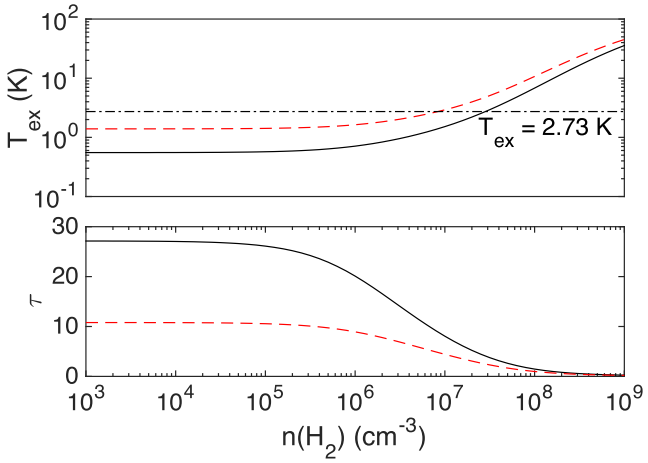

Figure 5. Excitation temperature (in K) and opacity of the OH transitions at 1.66 GHz obtained with the new rate coefficients (solid lines) and OHD94 rate coefficients (dashed lines) as a function of density. See the text for details.

temperature at low to intermediate densities ($n(H_2) < 10^8$ cm^{-3}). It is even interesting to note that the excitation temperature is below the CMB temperature for densities below 10^7 cm^{-3} so that the line could be detected in absorption against the CMB background. Both sets of collisional data predict such behaviour. It is however interesting to note that the use of the new rate coefficients predicts the line at 1.66 GHz to appear in emission ($T_{ex} > 2.73$ K) at a significantly larger density (1×10^7 cm^{-3} versus 3×10^7 cm^{-3}).

Since this line has been used for tracing the density (Cotten et al. 2012) of molecular cloud envelopes, we anticipate that the use of the new rate coefficients will affect significantly predictions of physical conditions deduced from OH observations. It is also interesting to see that the opacity of the line at 1.66 GHz obtained from the two sets of collisional data is substantially different: the opacity predicted from the new set being significantly larger, especially at low to intermediate densities (10^3–10^7 cm^{-3}). This is a direct consequence of the overall larger size of the new rate coefficients.

Finally, we note that the hyperfine structure of OH transitions is resolved in many interstellar sources (e.g. Wampfler et al. 2011; Ebisawa et al. 2015). As discussed above, the hyperfine structure of OH was neglected in the present calculations but will be included in a forthcoming publication by means of the 'exact' spin-recoupling technique, as in OHD94. Hyperfine-resolved rate coefficients could also be estimated from the present rotational/fine-structure rate coefficients by means of the so-called statistical or proportional approach ('M_j randomizing limit'). Here, one assumes that the hyperfine deexcitation rate coefficients are proportional to the degeneracy $(2F' + 1)$ of the final hyperfine level (and independent of the initial hyperfine level):

$$k_{^2\Pi_\Omega, j, p, F, j_2 \rightarrow {}^2\Pi_{\Omega'}, j', p', F', j_2'} = \frac{(2F'+1)}{(2I+1)(2j'+1)} k_{^2\Pi_\Omega, j, p, j_2 \rightarrow {}^2\Pi_{\Omega'}, j', p', j_2'}, \quad (3)$$

where $I = 1/2$ is the nuclear spin of the hydrogen atom and where each hyperfine level is designated by a quantum number F ($\mathbf{F} = \mathbf{I} + \mathbf{j}$). Unfortunately, this method is however known to be unreliable because it does not predict the known propensity rule $\Delta j = \Delta F$, predicted both theoretically and seen in experiment (Alexander & Dagdigian 1985). As shown by Faure & Lique (2012), propensity rules become important in radiative transfer computations whenever the opacity of the lines increases.

In addition, in the case of the modelling of the OH transition at 1.66 GHz, we also expect a strong temperature dependence due to the influence of the $^2\Pi_{3/2}, j = 5/2, p = +/-$ and $^2\Pi_{1/2}, j = 1/2, p = +/-$ levels that will be significantly populated only at temperature above ∼50 K. We will present hyperfine-resolved 'recoupling' rate coefficients in a future work where we will discuss in particular the anomalies and population inversions of the four hyperfine components of the 1.66 GHz transition.

5 CONCLUSION

We have computed a new set of fine-structure resolved rate coefficients for the OH–H_2 collisional system based on an accurate set of PESs. The state-to-state rate coefficients will be made available in the LAMDA (Schöier et al. 2005) and BASECOL (Dubernet et al. 2013) data bases. We have found that the new OH–H_2 rate coefficients are significantly larger than those currently used for astrophysical modelling. Consequently, we recommend this new set in modelling OH emission from molecular clouds.

In order to evaluate the effect of these new data in astrophysical modelling, we have performed radiative transfer calculations corresponding to typical physical conditions of the ISM where OH emission is detected. In cold molecular clouds, the simulated brightness temperatures obtained with our new rate coefficients are very similar to the ones obtained with previous rate coefficients because LTE conditions are fulfilled. In star-forming regions, the simulated brightness temperatures obtained with our new rate coefficients are larger than the ones obtained with previous rate coefficients reflecting the differences seen in the rate coefficients. As a consequence, the use of the present rate coefficients will predict a significantly reduced OH abundance.

We plan to extend the present calculations to consider the hyperfine structure of the OH molecule in order to provide the astrophysical community with all the kinetic data necessary for the accurate modelling of the observations of OH and to account fully for the maser emission that is frequently seen in OH spectra.

ACKNOWLEDGEMENTS

We acknowledge financial support from the U.S. National Science Foundation, Grant No. CHE-1565872. J. K. acknowledges XSEDE.org Grant No. CHE-130120 and University of Maryland High-Performance Deepthought facilities for computational time. F. L. and A. F. acknowledge the Agence Nationale de la Recherche (ANR-HYDRIDES), contract ANR-12-BS05-0011-01.

REFERENCES

Alexander M. H., Dagdigian P. J., 1985, J. Chem. Phys., 83, 2191
Cotten D. L., Magnani L., Wennerstrom E. A., Douglas K. A., Onello J. S., 2012, AJ, 144, 163
Crutcher R. M., 2012, ARA&A, 50, 29
Dubernet M. L. et al., 2013, A&A, 553, A50
Ebisawa Y., Inokuma H., Sakai N., Menten K. M., Maezawa H., Yamamoto S., 2015, ApJ, 815, 13
Faure A., Lique F., 2012, MNRAS, 425, 740
Gerin M., Neufeld D. A., Goicoechea J. R., 2016, ARA&A, 54, 181
Goicoechea J. R. et al., 2011, A&A, 530, L16
Groenenboom G. C., Fishchuk A. V., van der Avoird A., 2009, J. Chem. Phys., 131, 124307
Harju J., Winnberg A., Wouterloot J. G. A., 2000, A&A, 353, 1065

Hibridon, 2012, is a package of programs for the time-independent quantum treatment of inelastic collisions and photodissociation written by M. H. Alexander, D. E. Manolopoulos, H.-J. Werner, B. Follmeg, P. J. Dagdigian, and others. More information and/or a copy of the code can be obtained from the website http://www2.chem.umd.edu/groups/alexander/hibridon
Huber K. P., Herzberg G., 1979, Molecular Spectra and Molecular Structure. IV. Constants of Diatomic Molecules. Van Nostrand Reinhold, New York
Keto E., Rybicki G., 2010, ApJ, 716, 1315
Kochanski E., Flower D. R., 1981, Chem. Phys., 57, 217
Loomis R. A., Schwarz R. L., Lester M. I., 1996, J. Chem. Phys., 104, 6984
Ma Q., Kłos J. Alexander M. H., van der Avoird A., Dagdigian P. J., 2014, J. Chem. Phys., 141, 174309
Mélen F., Sauval A. J., Grevesse N., Farmer C. B., Servais Ch., Delbouille L., Roland G., 1995, J. Mol. Spectrosc., 174, 490
Offer A., Flower D. R., 1990, J. Phys. B: At. Mol. Opt. Phys., 23, L391
Offer A. R., van Dishoeck E. F., 1992, MNRAS, 257, 377
Offer A. R., van Hemert M. C., 1993, J. Chem. Phys., 99, 3836
Offer A. R., van Hemert M. C., van Dishoeck E. F., 1994, J. Chem. Phys., 100, 362
Roueff E., Lique F., 2013, Chem. Rev., 113, 8906
Schewe H. C. et al., 2015, J. Chem. Phys., 142, 204310
Schöier F. L., van der Tak F. F. S., van Dishoeck E. F., Black J. H., 2005, A&A, 432, 369
Shannon R. J., Blitz M. A., Goddard A., Heard D. E., 2013, Nat. Chem., 5, 745
van der Tak F. F. S., Black J. H., Schöier F. L., Jansen D. J., van Dishoeck E. F., 2007, A&A, 468, 627
Wakelam V. et al., 2015, ApJS, 217, 20
Wampfler S. F. et al., 2011, A&A, 531, L16
Wampfler S. F. et al., 2013, A&A, 552, A56
Weinreb S., Barrett A. H., Meeks M. L., Henry J. C., 1963, Nature, 200, 829

This paper has been typeset from a TEX/LATEX file prepared by the author.